Modelling ADF STEM images using elliptical Gaussian peaks and its effects on the quantification of structure parameters in the presence of sample tilt

Modelling ADF STEM images using elliptical Gaussian peaks and its effects on the quantification of structure parameters in the presence of sample tilt

Annelies De wael[a,b], Annick De Backer[a,b], Ivan Lobato[a,b], Sandra Van Aert[a,b,*]

[a]*EMAT, University of Antwerp, Groenenborgerlaan 171, 2020 Antwerp, Belgium*
[b]*NANOlab Center of Excellence, University of Antwerp, Belgium*

Abstract

A small sample tilt away from a main zone axis orientation results in an elongation of the atomic columns in ADF STEM images. An often posed research question is therefore whether the ADF STEM image intensities of tilted nanomaterials should be quantified using a parametric imaging model consisting of elliptical rather than the currently used symmetrical peaks. To this purpose, simulated ADF STEM images corresponding to different amounts of sample tilt are studied using a parametric imaging model that consists of superimposed 2D elliptical Gaussian peaks on the one hand and symmetrical Gaussian peaks on the other hand. We investigate the quantification of structural parameters such as atomic column positions and scattering cross sections using both parametric imaging models. In this manner, we quantitatively study what can be gained from this elliptical model for quantitative ADF STEM, despite the increased parameter space and computational effort. Although a qualitative improvement can be achieved, no significant quantitative improvement in the estimated structure parameters is achieved by the elliptical model as compared to the symmetrical model. The decrease in scattering cross sections with increasing sample tilt is even identical for both types of parametric imaging models. This impedes direct comparison with zone axis image simulations. Nonetheless, we demonstrate how reliable atom-counting can still be achieved in the presence of small sample tilt.

Keywords: quantitative electron microscopy, sample tilt, scanning transmission electron microscopy, statistical parameter estimation theory, elliptical imaging model

1. Introduction

The properties of nanomaterials are strongly dependent on their size and shape, as well as on their composition and the positions of the individual atoms [1, 2, 3, 4, 5, 6]. This implies that unravelling the structure-properties relationship of nanomaterials requires an accurate and precise quantification of the atomic structure. Therefore, quantitative rather than qualitative analysis of annular dark field (ADF) scanning transmission electron microscopy (STEM) images is becoming a recognised approach [7, 8, 9, 10, 11]. The image intensities in ADF STEM images of crystalline nanomaterials are strongly peaked at the atomic column positions. Furthermore, due to the incoherent nature of the image intensities in ADF STEM - provided that the annular detector inner angle is chosen sufficiently large - the contrast in the ADF STEM images is sensitive to the atomic number Z of the atoms in the nanomaterials, as well as to the thickness of the nanomaterial [12, 13, 14, 15]. Different approaches for quantitative interpretation of ADF STEM images exist. Either the image intensities are directly compared to image simulations, or an approach based on statistical parameter estimation theory can be followed. When experimental image intensities are directly compared to image simulations on a pixel-by-pixel basis, an accurate and precise knowledge of all microscope parameters such as detector efficiency and aberrations is crucial [16, 17]. Therefore, image intensities from the experimental ADF STEM image should first be put on an absolute scale, such that they are normalised with respect to the incident electron beam, and detector efficiency is accounted for [18, 19, 20]. The robustness to microscope aberrations as well as the sensitivity to thickness improves significantly when the total intensity scattered from each atomic column is used as a measure for quantification, rather than the individual pixels or the peak intensities [8, 21, 22, 23]. This integrated intensity is the so-called scattering cross section and can be quantified by integrating the intensities in a Voronoi cell around the atomic column positions [21]. Alternatively, a parametric imaging model consisting of a superposition of two-dimensional (2D) Gaussian peaks can be fitted to the image intensities [8, 24]. The scattering cross sections are then quantified by the volumes under the 2D Gaussian peaks. The scattering cross sections have been used to determine the composition of nanomaterials [8, 25], and to count the number of atoms in each atomic column of monatomic [26, 27, 28, 29, 30, 31, 32, 33] and mixed element [34, 35] nanomaterials. Furthermore, the parametric imaging model provides precise estimates for the atomic

*sandra.vanaert@uantwerpen.be

column positions with a precision that surpasses the spatial resolution limit of the electron microscope [11, 24]. When the electron dose is low, it becomes more challenging to correctly identify all atomic columns present in the ADF STEM image. In such case, the maximum *a posteriori* (MAP) probability rule can be used to reliably detect each atomic column [36, 37].

The aforementioned parametric imaging model was developed for quantitative analysis of ADF STEM images of nanomaterials in zone axis orientation. However, aligning the sample in exact zone axis orientation might not always be possible for various reasons, such as sample bending in very thin specimens [38]. Many interesting nanoparticles, for example for catalytic applications, are very small and therefore rotate under the influence of the electron beam, which leads to small amounts of sample tilt [39, 40]. This can affect the quantification of the atomic structure from the ADF STEM image intensities [31]. The effects of tilt on high resolution ADF STEM images have been studied using multislice calculations [41, 42], revealing that the contrast between background and bright column intensities is decreased when the specimen is tilted slightly off zone-axis orientation. This can be explained using electron channelling theory [21, 43, 44, 45]. An atomic column aligned with the incident beam exhibits a small lensing effect on the beam, keeping the intensity on the atomic column [34, 35, 43, 44]. This leads to a larger scattering cross section than the sum of the individual scattering cross sections of the separate atoms in the atomic column. Tilting the sample away from zone axis orientation reduces the channelling and leads to a decrease in the intensity scattered from the atomic column towards the annular detector, as compared to the zone axis oriented situation [21, 45, 46, 47, 48]. Nonetheless, the crystal lattice remains clearly visible for specimen tilts up to one degree in different directions and for a range of specimen thicknesses. While acquiring images, tilt can therefore remain unnoticed despite the decrease in contrast, as the intensity range displayed when acquiring the images is rescaled [9]. Empirically, sample tilt also causes an elongation of the atomic columns in the ADF STEM images. In our experience, an often posed research question is therefore whether the parametric imaging model consisting of symmetrical Gaussian peaks can still yield a reliable quantification. Quantitative ADF STEM in the presence of sample tilt was previously studied by estimating scattering cross sections using the integrated intensity in Voronoi cells [45]. However, the scattering cross sections are estimated more reliably when overlap between neighbouring atomic columns is taken into account [24]. In a tilted specimen, these overlapping intensities will become even more important, and a parametric imaging model consisting of overlapping peaks to model the expected values of the ADF STEM intensities is essential. The Gaussian peaks were shown to provide an adequate description of the experimental ADF STEM image intensities [24, 49, 50]. We therefore propose to use 2D elliptical Gaussian peaks rather than 2D symmetrical Gaussian peaks, in order to better describe the elongated ADF STEM image intensities in the presence of sample tilt. In this paper, we investigate whether physical parameters such as scattering cross sections or atomic column positions can be estimated more reliably using a parametric imaging model that consists of superimposed 2D elliptical Gaussian peaks. In Section 2, the proposed parametric imaging model is introduced. In Section 3, the possibilities and limitations of the elliptical imaging model are studied using simulated ADF STEM images of hypothetical Pt(110) nanocrystals with various amounts of sample tilt. The amount of elongation of the atomic columns is quantified by the elliptical model and the effect of sample tilt on the estimated atomic column positions, intercolumn distance and scattering cross sections is studied using the proposed elliptical model and compared to the results obtained using the existing symmetrical model. In Section 4, the most reliable strategy for atom-counting from tilted nanomaterials is discussed using simulated ADF STEM images of a hypothetical Pt nanoparticle. Finally, in Section 5, the results are discussed and conclusions are drawn.

2. Parametric imaging model

In previous work, a quantitative model to describe the ADF STEM image intensities has been introduced using overlapping 2D symmetrical Gaussian peaks [8, 24, 29]. To this purpose, the pixel values w_{kl} for each pixel (k, l) of a $K \times L$ ADF STEM image are summarised in a vector:

$$\mathbf{w} = (w_{11}, w_{12}, \cdots, w_{KL}). \tag{1}$$

This is the set of observations obtained from the ADF STEM experiment. Each set of observations obtained from an experiment performed under the same experimental conditions will unavoidably be different due to the presence of noise. Therefore, the pixel intensities are stochastic variables. The expectation value $\mathbb{E}[w_{kl}]$ of the ADF STEM image intensity at pixel (k, l) is then given by:

$$f_{kl}(\boldsymbol{\theta}) = \zeta + \sum_{n=1}^{N} \eta_n \exp\left(-\frac{(x_k - \beta_{x_n})^2 + (y_l - \beta_{y_n})^2}{2\rho^2}\right). \tag{2}$$

In this expression, ζ is a constant background present in the image, η_n is the height of the n^{th} Gaussian peak, β_{x_n} and β_{y_n} are the x- and y-coordinate of the n^{th} atomic column, ρ is the width of the 2D symmetrical Gaussian peaks fitted to all atomic columns and N is the total number of atomic columns. The $3N + 2$ unknown parameters are summarised in the parameter vector:

$$\boldsymbol{\theta} = (\beta_{x_1}, \cdots, \beta_{x_N}, \beta_{y_1}, \cdots, \beta_{y_N}, \eta_1, \cdots, \eta_N, \zeta, \rho)^{\mathsf{T}}. \tag{3}$$

We will now elaborate on this parametric imaging model, by replacing the symmetrical Gaussian peaks with elliptical Gaussian peaks:

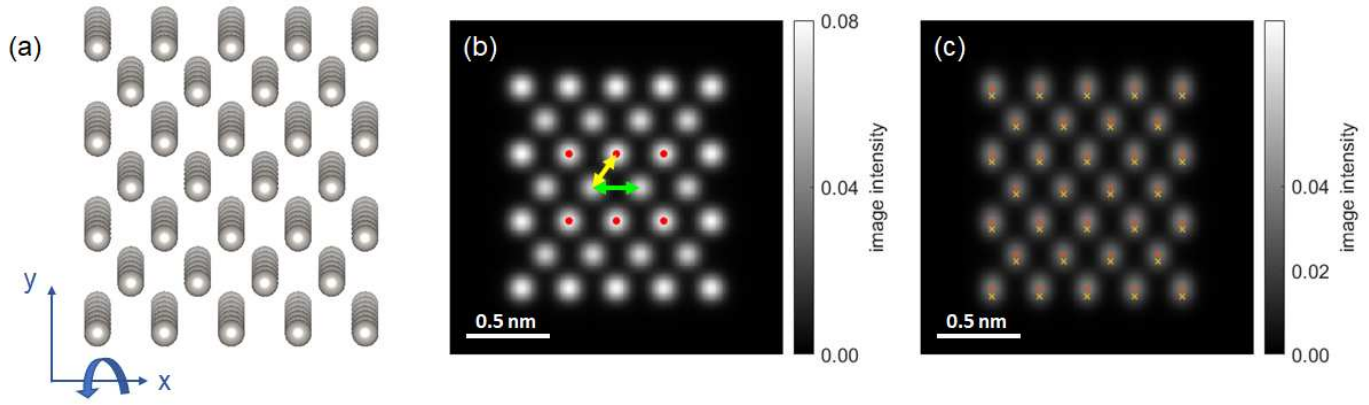

Figure 1: (a) Visualisation of the Pt(110) nanocrystal of 4×3 unit cells, with a thickness of 6 unit cells. The tilt direction used in the simulation study is shown schematically. (b) Simulated ADF STEM image of the Pt(110) nanocrystal in zone axis orientation. Red dots indicate the columns used to determine the position bias and scattering cross sections as a function of tilt in Fig. 4(a) and Fig. 5. The arrows indicate the columns for which the nearest and next nearest neighbour distance is assessed in Fig. 4(b). (c) Simulated ADF STEM image of the Pt(110) nanocrystal with a sample tilt of 16 mrad. Estimated and reference coordinates - discussed in Section 3.2 - are plotted on top of the image with red and yellow crosses respectively. Image intensities are expressed in fractions of the incident electron dose and are shown on the same colour scale. Colour bar labels indicate the minimum-maximum range present in the individual images.

$$f_{kl}(\mathbf{\Theta}) = \zeta + \sum_{n=1}^{N} \eta_n \exp\left(- \frac{[\cos\alpha\,(x_k - \beta_{x_n}) + \sin\alpha\,(y_l - \beta_{y_n})]^2}{2{\rho_x}^2} - \frac{[-\sin\alpha\,(x_k - \beta_{x_n}) + \cos\alpha\,(y_l - \beta_{y_n})]^2}{2{\rho_y}^2} \right). \quad (4)$$

In this expression, ρ_x and ρ_y are the widths in the x- and y-direction of the 2D elliptical Gaussian peaks fitted to all atomic columns and α is the angle that indicates the orientation of the elliptical Gaussian peaks. The $3N + 4$ unknown parameters are summarised in the parameter vector:

$$\mathbf{\Theta} = (\beta_{x_1}, \cdots, \beta_{x_N}, \beta_{y_1}, \cdots, \beta_{y_N}, \eta_1, \cdots, \eta_N, \zeta, \rho_x, \rho_y, \alpha)^{\mathsf{T}}. \quad (5)$$

In the case of an untilted sample, it is preferable to keep the width constant per atom type, as in Eq. (2), in order to improve the robustness of the fit. Fitting a different width for each atomic column increases the parameter space, and consequently reduces the precision of the parameter estimates. In the case of a tilted sample, this assumption remains a valid choice when there are only small thickness variations present in the sample. In this case, fitting with a constant width in the x- and y-direction respectively, as in Eq. (4), yields the most precise parameter estimates, since in this manner, the parameter space is smaller. However, sample tilt causes a larger elongation of thicker atomic columns in the ADF STEM image, and therefore this assumption is no longer accurate when fitting a sample with a large variation in sample thickness. In this case, each atomic column should be fitted using a different width for the 2D elliptical Gaussian peaks:

$$f_{kl}(\mathbf{\Theta}) = \zeta + \sum_{n=1}^{N} \eta_n \exp\left(- \frac{[\cos\alpha\,(x_k - \beta_{x_n}) + \sin\alpha\,(y_l - \beta_{y_n})]^2}{2{\rho_{x_n}}^2} - \frac{[-\sin\alpha\,(x_k - \beta_{x_n}) + \cos\alpha\,(y_l - \beta_{y_n})]^2}{2{\rho_{y_n}}^2} \right), \quad (6)$$

with ρ_{x_n} and ρ_{y_n} the widths in the x- and y-direction of the 2D elliptical Gaussian peak fitted to the n^{th} atomic column. The $5N+2$ unknown parameters are summarised in the parameter vector:

$$\mathbf{\Theta} = (\beta_{x_1}, \cdots, \beta_{x_N}, \beta_{y_1}, \cdots, \beta_{y_N}, \eta_1, \cdots, \eta_N, \zeta, \rho_{x_1}, \cdots, \rho_{x_N}, \rho_{y_1}, \cdots, \rho_{y_N}, \alpha)^{\mathsf{T}}. \quad (7)$$

The angle α is kept constant, as sample tilt often occurs for the whole sample in the same direction. In case of a spatially varying tilting direction - for example due to sample bending in 2D nanomaterials, one could also estimate different angles for each column, although this will increase the parameter space even further. The selected parametric model is then fitted to the experimental ADF STEM image using a least squares criterion. In this manner we obtain a least squares estimate for the unknown parameter vector:

$$\hat{\mathbf{\Theta}} = \arg\min_{\mathbf{t}} \sum_{k=1}^{K} \sum_{l=1}^{L} (w_{kl} - f_{kl}(\mathbf{t}))^2. \quad (8)$$

3. Simulation study

We will now apply this new parametric imaging model to the quantification of ADF STEM images in the presence of sample tilt and compare the results to the quantification using the existing symmetrical Gaussian model. To this purpose, we simulated a Pt(110) nanocrystal with a sample tilt ranging from 0 to 60 mrad - approximately 3.5 degrees - towards a [100] zone axis orientation. We consider a nanocrystal with two different thicknesses, respectively 6 and 18 unit cells, corresponding to a total thickness of 16.64$\mathring{A}$ and 49.92$\mathring{A}$. The atomic structure of the Pt(110) nanocrystal at 6 unit cells thickness used for the simulation study is shown in Fig. 1(a). Fig. 1(b) and Fig. 1(c) show simulated ADF STEM images of the sample in zone axis orientation and with 60 mrad tilt towards a [100] zone axis orientation, respectively. The tilting direction is indicated schematically in Fig. 1(a). Sample tilt was included in the multislice simulations by using the transformed (x, y, z) coordinates of the atoms after rotation of the sample. For all tilt angles, a fixed height was used as a zero defocus reference plane, i.e. the z-height of the focussed electron probe when the defocus in the image simulations is equal to zero, in order to ensure a fair comparison of the images. The parameters of the image simulations are summarised in Table 1. Image simulations were performed using multiple frozen phonon configurations with displacements of the atoms determined by the Debye-Waller factor, in order to include thermal vibrations [51]. All multislice image simulations discussed in this paper were performed using MULTEM [52, 53]. The (untilted) nanocrystal is created with a homogeneous thickness by replicating the crystal unit cell in the x, y and z directions. As a result, there are two types of atomic columns in the nanocrystal, corresponding to the corners or the central atom of the projected unit cell of a face centered cubic (FCC) lattice. This leads to a variation in the number of atoms per atomic column of only 1 atom. Therefore, the elongation will be approximately the same for all atomic columns, and the images are fitted using the model with constant width for each direction, expressed by Eq. (4).

In Fig. 2, we display the residual intensities obtained by subtracting the simulated image intensities of the tilted Pt(110) nanocrystal [Fig. 1(c)] from the fitted image intensities using the symmetrical and the elliptical model respectively. By visualising the intensities on the same colour scale, we can now easily understand why one would want to consider fitting 2D elliptical Gaussian peaks: the residual intensities for this tilted Pt nanocrystal are up to a factor of 3.5 smaller as compared to the commonly used symmetrical model, yielding a qualitatively better description of the ADF STEM image intensities in the presence of sample tilt. In the remainder of this section we will quantitatively study whether this improvement can also yield better estimates of physical parameters such as atomic column positions and scattering cross sections. Furthermore, the model also provides an estimate for the angle, which can be used to determine the tilting direction. Based on the widths in the x and y direction of the 2D elliptical Gaussian peaks, we can study the elongation of the atomic columns, which is related to the amount of sample tilt.

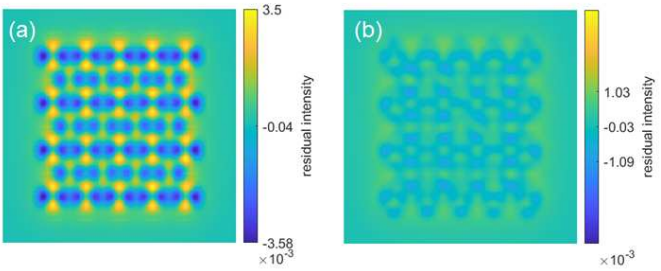

Figure 2: Residual intensities of the tilted Pt(110) nanocrystal from Fig. 1(c) after fitting with a superposition of (a) symmetrical and (b) elliptical 2D Gaussian peaks. Residual image intensities are expressed in fractions of the incident electron dose and are shown on the same colour scale. Colour bar labels indicate the minimum-maximum range present in the individual images.

3.1. Atomic column elongation

The elliptical model given by Eq. (4) allows us to quantify the amount of elongation visible in the tilted image using the aspect ratio of the ellips:

$$\epsilon = \frac{\rho_x}{\rho_y} \leq 1. \tag{9}$$

The aspect ratio is equal to or smaller than one by definition. This is achieved by consistently defining ρ_x as the smallest width of the ellips after the parameter estimation procedure. The aspect ratio ϵ decreases with increasing sample tilt. This is shown in Fig. 3 for the Pt(110) nanocrystal of Fig. 1. For a larger sample thickness, the aspect ratio decreases faster with increasing sample tilt. When the sample thickness is known, the combination of image simulation and elliptical fitting can be used to estimate the amount of sample tilt.

3.2. Atomic column positions

Next, we assess the accuracy of the estimated atomic column positions using the proposed elliptical parametric imaging model and compare this to the existing parametric model with symmetrical Gaussians. To this purpose, we quantify the bias of the position estimate for the atomic columns indicated by red dots in Fig. 1(b), which have the same z-height in the FCC crystal lattice. The results are summarised in Fig. 4(a) for different amounts of sample tilt and sample thickness. The bias of the position estimate is quantified as the distance between the reference coordinate and the estimated position coordinate. During this analysis, we have set the reference position of an atomic column in a tilted sample equal to the xy-position of the

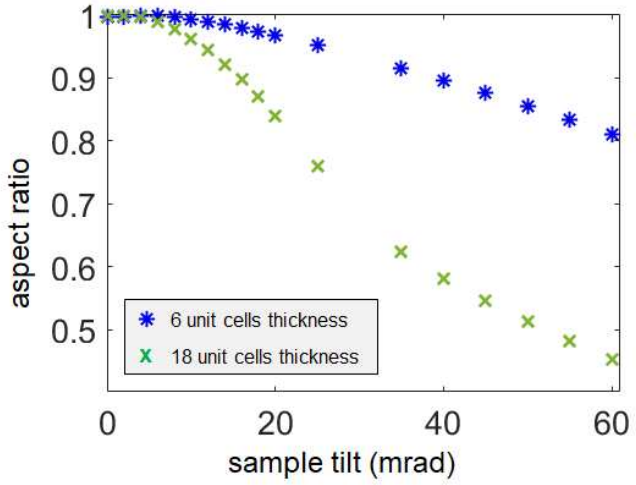

Figure 3: Aspect ratio ϵ of the atomic columns estimated using a parametric imaging model with elliptical Gaussian peaks, evaluated as a function of the amount of sample tilt for the Pt nanocrystal from Fig. 1, at 6 and 18 unit cells thickness ($16.64\mathring{A}$ and $49.92\mathring{A}$).

top atom of that atomic column. In Fig. 1(c), the estimated and reference coordinates are plotted on top of the image with red and yellow crosses respectively. A shift of the estimated atomic column positions as compared to the actual position of the top atoms occurs when the sample is tilted. This was noted before, especially for annular bright field (ABF) STEM images [42, 54, 55, 56]. The bias of the estimated atomic column positions increases with increasing sample tilt and sample thickness. At 18 unit cells thickness, for example, the bias on the estimated atomic column position is 11.4% of the nearest neighbour distance at a sample tilt of 16 mrad (approximately 1 degree). Despite this bias, the intercolumn distance is still estimated accurately, as shown in Fig. 4(b) for the thickness of 18 unit cells. The estimated intercolumn distance by the elliptical model differs at most 1.8 pm from the reference value. This enables us to reliably quantify the lattice parameter using the parametric imaging models.
Finally, we see that the accuracy of the estimated position coordinate and the intercolumn distance is identical for the parametric imaging model using symmetrical or elliptical 2D Gaussian peaks up to 50 mrad (almost 3 degrees) in case of 18 unit cells thickness (approximately 50 $\mathring{A}$). Only at larger tilt angles, the bias on the estimated intercolumn distances by the symmetrical model of 4.5 pm exceeds the bias obtained by the elliptical model. A drawback of the elliptical model on the other hand is the increased parameter space, which can lead to less precise parameter estimates [57, 58]. Therefore, when the goal is to quantify the atomic column positions from an ADF STEM image of a slightly tilted sample, we recommend to use the existing parametric imaging model, rather than increasing the complexity of the model.

3.3. Scattering cross sections

The total intensity scattered from an atomic column towards the annular detector is quantified by the so-called scattering cross section, which can be estimated by the volume under the 2D Gaussian peaks of the parametric imaging model given by Eq. (2) [8, 24, 29]. This volume is expressed as follows for each atomic column n:

$$\hat{V}_n = 2\pi\hat{\eta}_n\hat{\rho}^2. \tag{10}$$

As mentioned before, tilting of a sample away from zone axis orientation reduces the channeling effect, leading to a decrease in the contrast and in the peak intensity at the atomic column positions. This effect is indeed observed when we evaluate the scattering cross sections estimated according to Eq. (10) as a function of sample tilt, shown in Fig. 5. Note that, although image contrast can be altered using defocus, this does not affect the scattering cross sections, which are robust to defocus and other microscope aberrations [22].
One might expect that the elliptical model introduced in this paper yields more reliable estimates for the total scattered intensity from each column, since the model seems to empirically better describe the shape of the atomic columns of tilted nanomaterials in ADF STEM images, as was shown by the residual image intensities in Fig. 2. We therefore quantify the scattering cross sections from the elliptical model of Eq. (4) as well. The volumes under the elliptical Gaussian peaks are quantified in a similar manner to Eq. (10) as follows:

$$\hat{V}_n = 2\pi\hat{\eta}_n\hat{\rho}_x\hat{\rho}_y. \tag{11}$$

The estimated scattering cross sections from the proposed elliptical model as a function of sample tilt are shown in Fig. 5. Note that they are identical to the scattering cross sections estimated by the existing symmetrical model. In other words, both peak shapes succeed in accounting for the scattered intensity that originates from the atomic column, by adjusting height and width(s) accordingly. We therefore conclude that we do not gain extra intensity information by adapting the parametric imaging model using elliptical peaks.
Note that lens aberrations such as coma can also cause elongation of the atomic columns, which might potentially be mistaken as sample tilt [42]. It was however shown previously that the scattering cross section estimated from the parametric imaging model using 2D symmetrical Gaussian peaks is robust for inaccuracies in both cylindrically symmetrical and non-cylindrically symmetrical aberrations [23]. Therefore, we do not expect problems for the quantification of slightly aberrated ADF STEM images with the existing symmetrical Gaussian model.

4. Atom-counting in the presence of sample tilt

In this section, we demonstrate that, despite the decrease in the scattering cross sections discussed in Section 3.3,

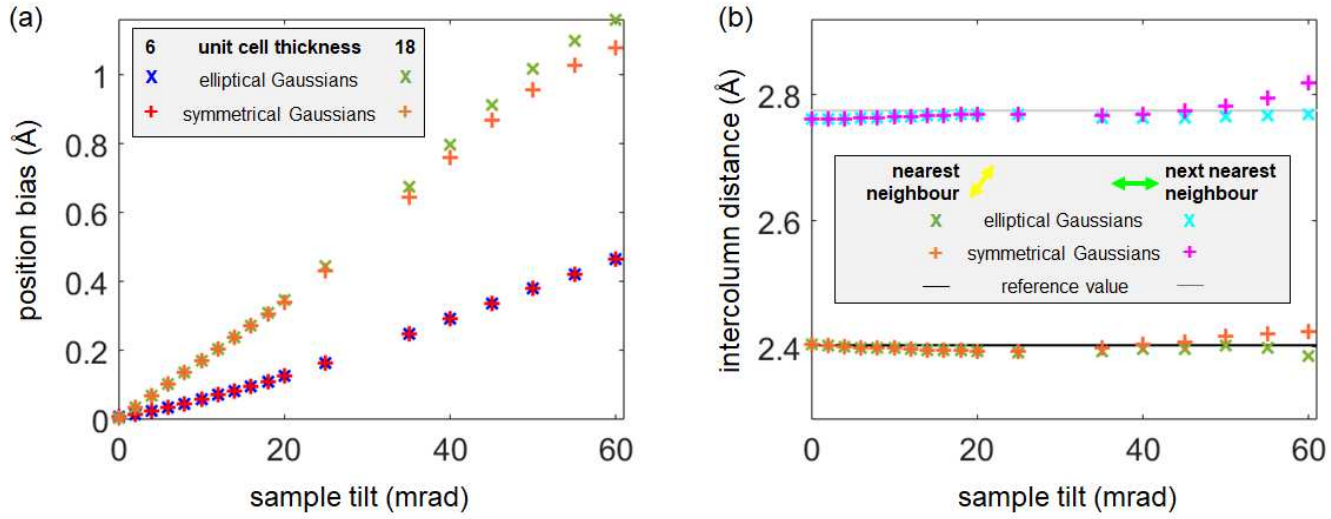

Figure 4: (a) Bias between the actual atomic column position - equal to the position of the top atom - and the atomic column position estimated using a parametric imaging model with elliptical and symmetrical Gaussian peaks, evaluated as a function of the amount of sample tilt. The bias was calculated for the atomic columns indicated with red dots in Fig. 1(b). (b) Distance between two nearest neighbour atomic columns and between two next nearest neighbour atomic columns, indicated respectively using a yellow and a green arrow in Fig. 1(b), estimated using a parametric imaging model with elliptical and symmetrical Gaussian peaks, evaluated as a function of the amount of sample tilt for the Pt nanocrystal at 18 unit cells thickness (49.92Å). Full lines indicate the reference value, determined from the lattice parameters.

atom-counting in the presence of sample tilt can be achieved in a reliable manner using a hybrid statistics-simulations based method for atom-counting, previously introduced in [33]. This hybrid method immediately incorporates prior knowledge from carefully performed zone axis image simulations in the statistical parameter estimation framework, and in this manner enables reliable atom-counting at lower electron doses and in the presence of small sample tilt. This is achieved by no longer freely estimating the average scattering cross section corresponding to an atomic column with g atoms, but putting them equal to

$$\mu_g = a\mathcal{M}_g, \tag{12}$$

with $\mathcal{M}_g$ the simulated scattering cross section corresponding to an atomic column with g atoms and a a linear scaling parameter. This scaling parameter is estimated and can therefore account for a small mismatch between experimental and simulated conditions, such as a slight difference in detector angles or sample mistilt.

In order to demonstrate reliable atom-counting in the presence of sample tilt, we simulated ADF STEM images of a hypothetical Pt nanoparticle for which the atomic structure is shown in Fig. 6(a). The number of atoms in each atomic column along the viewing direction used to simulate the ADF STEM images is visualised in Fig. 6(b). Images were simulated corresponding to zone axis orientation, shown in Fig. 6(c), and with different amounts of sample tilt, up to 35 mrad, shown in Fig. 6(d). The parameters of the image simulations are summarised in Table 1. The scattering cross sections for each atomic column of the Pt nanoparticle were estimated using the parametric imaging model with 2D symmetrical Gaussian peaks. Furthermore, we created a library of scattering cross sections with the same microscope settings, corresponding to a zone axis oriented Pt crystal. Note that the ADF STEM images are analysed without noise, i.e. at infinite dose. In this manner, we can evaluate how well the scaling parameter a, introduced in Eq. (12), can compensate for the sample tilt, without mixing the interpretation of the results with dose effects.

Fig. 7(a) evaluates the estimated scaling parameter as a function of the sample tilt, as well as the percentage of correctly counted atomic columns. The hybrid method achieves more than 95% correctly counted atomic columns, even in the presence of sample tilt. At all tilt angles, the small percentage of miscounted atomic columns corresponds to differences of plus or minus 1 atom at most, as shown in Fig. 7(b)-(e). As expected, the scaling parameter is estimated close to 1 for the zone axis orientation. Then, after a plateau at small tilt angles, similar to the results of [45], the scaling parameter decreases with increasing sample tilt. This demonstrates the applicability of the hybrid method for atom-counting in case of sample tilt.

In this manner, we are able to perform reliable atom-counting in the presence of sample tilt, using the scattering cross sections estimated by the parametric imaging model with 2D symmetrical Gaussian peaks. Optimisation of the imaging parameters such as probe convergence angle and collection angles of the annular detector can further aid to-

Parameter	Section 3	Section 4
Acceleration voltage	300 kV	200 kV
Spherical aberration C_s	1 nm	0 nm
Defocus C_1	$14.03\mathring{A}$	$0\mathring{A}$
Zero defocus reference plane	$10.82\mathring{A}$	$17.83\mathring{A}$
Specimen thickness	$16.64\mathring{A}$ & $49.92\mathring{A}$	$23.58\mathring{A}$
Simulation box size (xy)	$50 \times 50\mathring{A}^2$	$50.09 \times 50.11\mathring{A}^2$
Probe convergence angle α	21 mrad	22.48 mrad
Annular detector inner angle	70 mrad	51.73 mrad
Annular detector outer angle	180 mrad	248.41 mrad
Number of phonon configurations	50	30
Spatial incoherence of source FWHM	$1\mathring{A}$	$1\mathring{A}$
Pixel size of simulated image	$0.10\mathring{A}$	$0.125\mathring{A}$
Pixel size to sample atomic potential	$0.046\mathring{A}$	$0.039\mathring{A}$
Pixel size to sample reciprocal space	$0.02\mathring{A}^{-1}$	$0.02\mathring{A}^{-1}$
Maximum reciprocal lattice vector	$10.8\ \mathring{A}^{-1}$	$12.77\ \mathring{A}^{-1}$
Slice thickness	$1.39\mathring{A}$	$1.39\mathring{A}$
Debye-Waller factor [59]	$0.5705\mathring{A}^2$	$0.5705\mathring{A}^2$
Zone axis	[110]	[110]
Tilt axis	$[1\bar{1}0]$	$[1\bar{1}0]$
Rotation center	center of mass	center of mass

Table 1: Parameters used for the multislice simulations of the Pt(110) nanocrystal and Pt nanoparticle discussed in Sections 3 and 4.

wards a tilt-robust image quantification by balancing the contributions of elastic scattering and thermal diffuse scattering (TDS) to the ADF STEM signal [45].

5. Discussion and conclusions

In this paper, we investigated a parametric imaging model consisting of overlapping 2D elliptical Gaussian peaks. Our goal was to ascertain whether this model can quantify the ADF STEM images of slightly tilted nanomaterials more reliably than the existing parametric imaging model, which consists of overlapping 2D symmetrical Gaussian peaks. Intuitively, such an elliptical model might seem better suited for the description of the elongated atomic columns observed in tilted ADF STEM images. This can be clearly understood by visualising the residual intensities, i.e. the difference between the ADF STEM image intensities and the fitted intensities by the model. The elliptical model yields significantly smaller residual intensities as compared to the existing symmetrical model. Qualitatively, it can therefore be considered as a better model. On the other hand, the elliptical model is more complex, and therefore fitting the parameters is more time consuming, as compared to the symmetrical model. For the zone axis orientation image of Fig. 1(b), the elliptical fitting takes 2 times longer. At higher tilt angles, even more computation time is needed to fit the extra parameters. For the simulated image with sample thickness of 6 unit cells at a tilt angle of 60 mrad, shown in Fig. 1(c), fitting the elliptical model took 3 times longer than fitting the symmetrical model. For the sample thickness of 18 unit cells the time difference was even a factor of 6. Furthermore, an increased parameter space generally leads to less precise parameter estimates. Therefore, it is important to quantitatively study what can be gained from using this elliptical model for quantitative ADF STEM in terms of physical parameters. To this purpose, we investigated a simulated Pt(110) nanocrystal at different tilt angles and different thicknesses. A benefit of the elliptical model is that it allows us to quantify two properties of the tilted sample which are not quantified by the existing symmetrical model: the elongation of the atomic columns and the angle of the elongation. The angle quantifies the direction of sample tilt, while the elongation is strongly related to the amount of sample tilt. Furthermore, we have shown that the proposed elliptical model yields equivalent atomic column position estimates as compared to the existing symmetrical model for small amounts of sample tilt. Although the estimated atomic column positions are shifted with respect to the positions of the top atom of each atomic column, the intercolumn distances are quantified accurately. In this manner, both parametric imaging models can still be used to obtain reliable structural information from ADF STEM images of tilted nanomaterials. Finally, we quantified the scattering cross section at different tilt angles upto 60 mrad, or approximately 3.5 degrees, using both models. The scattering cross sections decrease with increasing sample tilt in the same manner, regardless whether they are estimated from the elliptical or the symmetrical model. This intensity loss is entirely caused by a loss of the channelling conditions, and cannot be (partially) retrieved by an elliptical Gaussian peak to

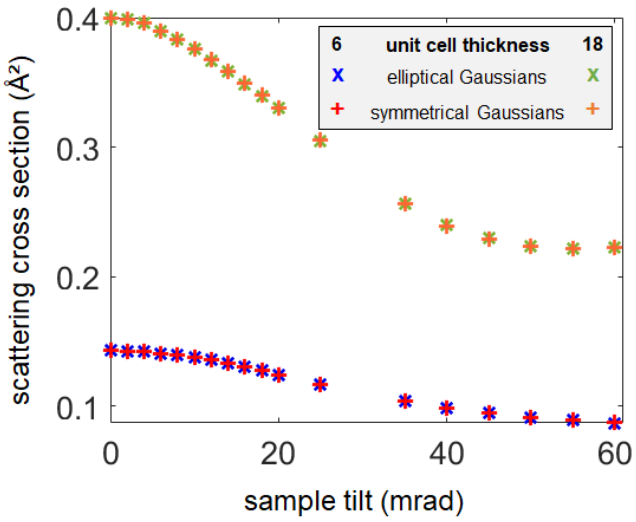

Figure 5: Scattering cross sections estimated using a parametric imaging model with elliptical and symmetrical Gaussian peaks, evaluated as a function of the amount of sample tilt, at 6 and 18 unit cells thickness (16.64$\AA$ and 49.92$\AA$). The scattering cross sections were estimated for the set of atomic columns indicated by the red dots in Fig. 1(b).

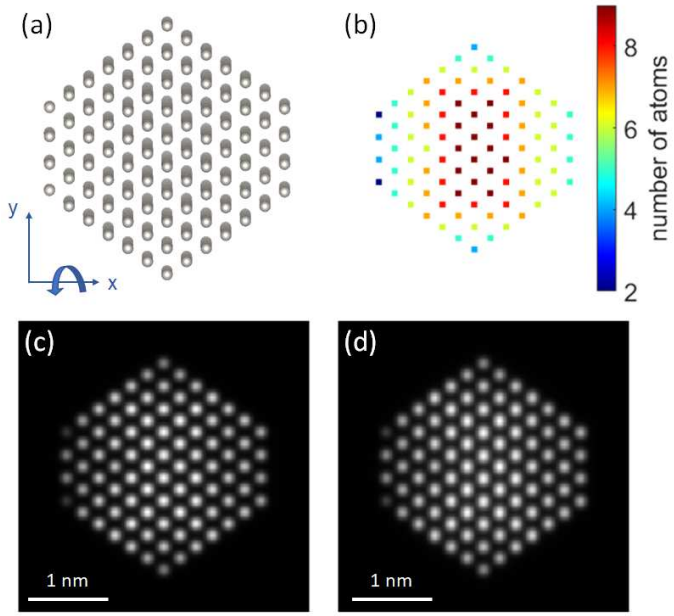

Figure 6: (a) Visualisation of the Pt nanoparticle. The tilt direction used in the simulation study is shown schematically. (b) Number of atoms in each atomic column along the viewing direction. (c) Simulated ADF STEM image of the Pt nanoparticle in zone axis orientation. (d) Simulated ADF STEM image of the Pt nanoparticle with a sample tilt of 35 mrad.

fit rather than a symmetrical Gaussian peak.
This implies that the scattering cross sections from tilted nanomaterials cannot be used to count the number of atoms using a simulations-based atom-counting procedure. The statistics-based approach for atom-counting on the other hand might still reveal a correct clustering of the scattering cross sections corresponding to atomic columns having the same thickness, but the unavoidable mismatch with the independent image simulations impedes truly reliable atom-counting in the presence of tilt. Therefore, the best approach is to use the hybrid statistics-simulations based atom-counting procedure [33], since this model explicitly allows for the existence of a mismatch due to sample tilt in the experimental and simulated scattering cross sections. Indeed, we show that reliable atom-counting is even possible in the presence of sample tilt using the hybrid method, owing to the scaling parameter that compensates for the lost intensity due to sample tilt.
In conclusion, we do not consider fitting the larger parameter space of the model with overlapping 2D elliptical Gaussian peaks worth the extra effort over fitting the existing model of overlapping 2D symmetrical Gaussian peaks, since we do not gain more reliable quantitative estimates for the atomic column positions and scattering cross sections. The comparison shown in this paper confirms that the existing parametric imaging model - which consists of overlapping 2D symmetrical Gaussian peaks - remains a very reliable method for the quantitative analysis of ADF STEM images in the presence of sample tilt. Correct lattice parameters can still be retrieved using the estimated atomic column positions. The scattering cross sections decrease with sample tilt, but an increased complexity of the parametric model does not help to retrieve (part of) this intensity loss. In short, we advise the use of overlapping 2D Gaussian peaks - previously implemented in the freely available StatSTEM software [24] - for the quantification of the ADF STEM image intensities, even in the presence of a small amount of sample tilt.

Acknowledgments

This project has received funding from the European Research Council (ERC) under the European Union's Horizon 2020 research and innovation programme (Grant Agreement No. 770887 and No. 823717 ESTEEM3). The authors acknowledge financial support from the Research Foundation Flanders (FWO, Belgium) through grants to A.D.w. and A.D.B. and projects G.0502.18N, G.0267.18N, and EOS 30489208. S.V.A. acknowledges TOP BOF funding from the University of Antwerp.

References

[1] J.-P. Locquet, J. Perret, J. Fompeyrine, E. Mächler, J. W. Seo, G. Van Tendeloo, Doubling the critical temperature of la1.9sr0.1cuo4 using epitaxial strain, Nature 394 (1998) 453–456.
[2] G. B. Olson, Designing a New Material World, Science 288 (2000) 993–998.

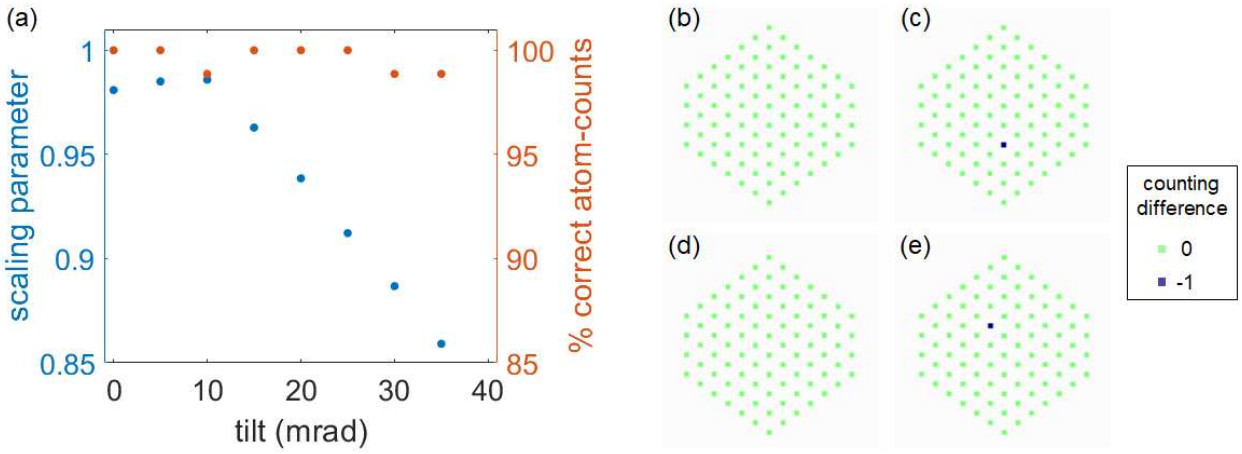

Figure 7: (a) Estimated scaling parameter and percentage of correctly counted atomic columns using the hybrid method for atom-counting from simulated ADF STEM images of the hypothetical Pt nanoparticle shown in Fig. 6, evaluated as function of sample tilt. (b-d) Difference counts as compared to the ground truth (Fig. 6(b)) at 0, 10, 25 and 35 mrad sample tilt respectively.

[3] N. Tian, Z.-Y. Zhou, S.-G. Sun, Y. Ding, Z. L. Wang, Synthesis of Tetrahexahedral Platinum Nanocrystals with High-Index Facets and High Electro-Oxidation Activity, Science 316 (2007) 732–735.

[4] J. Thomas, Tens of thousands of atoms replaced by one, Nature 525 (2015) 325–326.

[5] C. Wade, I. MacLaren, R. Vinci, M. Watanabe, The Role of Grain Boundary Dislocations in the Segregation-Induced Grain Boundary Embrittlement of Copper by Bismuth, Microscopy and Microanalysis 22 (2016) 1264–1265.

[6] R. Egerton, M. Watanabe, Characterization of single-atom catalysts by EELS and EDX spectroscopy, Ultramicroscopy 193 (2018) 111–117.

[7] J. M. LeBeau, S. D. Findlay, L. J. Allen, S. Stemmer, New Approach to Quantitative ADF STEM, Springer, Berlin, Heidelberg, 2008.

[8] S. Van Aert, J. Verbeeck, R. Erni, S. Bals, M. Luysberg, D. Van Dyck, G. Van Tendeloo, Quantitative atomic resolution mapping using high-angle annular dark field scanning transmission electron microscopy, Ultramicroscopy 109 (2009) 1236–1244.

[9] L. Jones, Quantitative ADF STEM: acquisition, analysis and interpretation, IOP Conf. Series: Materials Science and Engineering 109 (2016) 012008.

[10] S. Van Aert, A. De Backer, G. T. Martinez, A. J. den Dekker, D. Van Dyck, S. Bals, G. Van Tendeloo, Advanced electron crystallography through model-based imaging, IUCrJ 3 (2016) 71–83.

[11] A. De Backer, J. Fatermans, A. den Dekker, S. Van Aert, Quantitative Atomic-Resolution Electron Microscopy, Vol. 217 of Advances in Imaging and Electron Physics, 2021.

[12] P. D. Nellist, S. J. Pennycook, The Principles and Interpretation of Annular Dark-Field Z-Contrast Imaging, Advances in Imaging and Electron Physics 113 (2000) 147.

[13] S. J. Pennycook, L. A. Boatner, Chemically sensitive structure-imaging with a scanning transmission electron microscope, Nature 336 (1988) 565–567.

[14] J. M. Cowley, M. S. Hansen, S. Y. Wang, Imaging modes with an annular detector in STEM, Ultramicroscopy 58 (1995) 18–24.

[15] P. Hartel, D. Rose, C. Dinges, Conditions and reasons for incoherent imaging in STEM, Ultramicroscopy 63 (1996) 63–114.

[16] J. M. LeBeau, S. Stemmer, Experimental Quantification of Annular Dark-Field Images in Scanning Transmission Electron Microscopy, Ultramicroscopy 108 (2008) 1653–1658.

[17] C. Dwyer, C. Maunders, C. L. Zheng, M. Weyland, P. C. Tiemeijer, J. Etheridge, Sub-0.1 nm-resolution quantitative scanning transmission electron microscopy without adjustable parameters, Applied Physics Letters 100 (2012) 191915.

[18] S. D. Findlay, J. M. LeBeau, Detector non-uniformity in scanning transmission electron microscopy, Ultramicroscopy 124 (2013) 52–60.

[19] G. T. Martinez, L. Jones, A. De Backer, A. Béché, J. Verbeeck, S. Van Aert, P. Nellist, Quantitative STEM normalisation: The importance of the electron flux, Ultramicroscopy 159 (2015) 46–58.

[20] F. Krause, M. Schowalter, T. Grieb, K. Müller-Caspary, T. Mehrtens, A. Rosenauer, Effects of instrument imperfections on quantitative scanning transmission electron microscopy, Ultramicroscopy 161 (2016) 146–160.

[21] H. E, K. E. MacArthur, T. J. Pennycook, E. Okunishi, A. J. D'Alfonso, N. R. Lugg, L. J. Allen, P. D. Nellist, Probe integrated scattering cross sections in the analysis of atomic resolution HAADF STEM images, Ultramicroscopy 133 (2013) 109–119.

[22] G. T. Martinez, A. De Backer, A. Rosenauer, J. Verbeeck, S. Van Aert, The effect of probe inaccuracies on the quantitative model-based analysis of high angle annular dark field scanning transmission electron microscopy images, Micron 63 (2014) 57–63.

[23] G. T. Martinez, K. H. W. van den Bos, M. Alania, P. D. Nellist, S. Van Aert, Thickness dependence of scattering cross-sections in quantitative scanning transmission electron microscopy, Ultramicroscopy 187 (2018) 84–92.

[24] A. De Backer, K. H. W. van den Bos, W. Van den Broek, J. Sijbers, S. Van Aert, StatSTEM: An efficient approach for accurate and precise model-based quantification of atomic resolution electron microscopy images, Ultramicroscopy 171 (2016) 104–116.

[25] G. T. Martinez, A. Rosenauer, A. De Backer, J. Verbeeck, S. Van Aert, Quantitative composition determination at the atomic level using model-based high-angle annular dark field scanning transmission electron microscopy, Ultramicroscopy 137 (2014) 12–19.

[26] J. M. LeBeau, S. D. Findlay, L. J. Allen, S. Stemmer, Standardless atom counting in scanning transmission electron microscopy, Nano Letters 10 (2010) 4405–4408.

[27] S. Van Aert, K. J. Batenburg, M. D. Rossell, R. Erni, G. Van Tendeloo, Three-dimensional atomic imaging of crys-

talline nanoparticles, Nature 470 (2011) 374–377.
[28] S. Van Aert, A. De Backer, G. T. Martinez, B. Goris, S. Bals, G. Van Tendeloo, A. Rosenauer, Procedure to count atoms with trustworthy single-atom sensitivity, Physical Review B 87 (2013) 064107.
[29] A. De Backer, G. T. Martinez, A. Rosenauer, S. Van Aert, Atom counting in HAADF STEM using a statistical model-based approach: Methodology, possibilities, and inherent limitations, Ultramicroscopy 134 (2013) 23–33.
[30] L. Jones, K. E. MacArthur, V. T. Fauske, A. T. J. van Helvoort, P. D. Nellist, Rapid estimation of catalyst nanoparticle morphology and atomic-coordination by high-resolution Z-contrast electron microscopy, Nano Letters 14 (2014) 6336–6341.
[31] A. De Backer, G. T. Martinez, K. E. MacArthur, L. Jones, A. Béché, P. D. Nellist, S. Van Aert, Dose limited reliability of quantitative annular dark field scanning transmission electron microscopy for nano-particle atom-counting, Ultramicroscopy 151 (2015) 56–61.
[32] A. De Backer, A. De wael, J. Gonnissen, S. Van Aert, Optimal experimental design for nano-particle atom-counting from high-resolution stem images, Ultramicroscopy 151 (2015) 46–55.
[33] A. De wael, A. De Backer, L. Jones, P. D. Nellist, S. Van Aert, Hybrid statistics-simulations based method for atom-counting using scanning transmission electron microscopy, Ultramicroscopy 177 (2017) 69–77.
[34] K. H. W. van den Bos, A. De Backer, G. T. Martinez, N. Winckelmans, S. Bals, P. D. Nellist, S. Van Aert, Unscrambling Mixed Elements using High Angle Annular Dark Field Scanning Transmission Electron Microscopy, Physical Review Letters 116 (2016) 246101.
[35] K. H. W. van den Bos, L. Janssens, A. De Backer, S. Van Aert, The atomic lensing model: New opportunities for atom-by-atom metrology of heterogeneous nanomaterials, Ultramicroscopy 203 (2019) 155–162.
[36] J. Fatermans, A. J. den Dekker, K. Müller-Caspary, I. Lobato, C. M. O'Leary, P. D. Nellist, S. Van Aert, Single Atom Detection from Low Contrast-to-Noise Ratio Electron Microscopy Images, Physical Review Letters 121 (2018) 056101.
[37] J. Fatermans, S. Van Aert, A. J. den Dekker, The maximum a posteriori probability rule for atom column detection from HAADF STEM images, Ultramicroscopy 201 (2019) 81–91.
[38] H. G. Brown, R. Ishikawa, G. Sánchez-Santolino, N. R. Lugg, Y. Ikuhara, A. L. J., N. Shibata, A new method to detect and correct sample tilt in scanning transmission electron microscopy bright-field imaging, Ultramicroscopy 173 (2017) 76–83.
[39] Z. Y. Li, N. P. Young, M. Di Vece, S. Palomba, R. E. Palmer, A. L. Bleloch, B. C. Curley, R. L. Johnston, J. Jiang, J. Yuan, Three-dimensional atomic-scale structure of size-selected gold nanoclusters, Nature 451 (2008) 46–48.
[40] T. Altantzis, I. Lobato, A. De Backer, A. Béché, Y. Zhang, S. Basak, M. Porcu, Q. Xu, A. Sánchez-Iglesias, L. M. Liz-Marzán, G. Van Tendeloo, S. Van Aert, S. Bals, Three-Dimensional Quantification of the Facet Evolution of Pt Nanoparticles in a Variable Gaseous Environment, Nano Letters 19 (2019) 447–481.
[41] S. E. Maccagnano-Zacher, K. A. Mkhoyan, E. J. Kirkland, J. Silcox, Effects of tilt on high-resolution ADF-STEM imaging, Ultramicroscopy 108 (2008) 718–726.
[42] Y.-G. So, K. Kimoto, Effect of specimen misalignment on local sturcture analysis using annular dark-field imaging, Journal of Electron Microscopy 61 (2012) 207–215.
[43] R. F. Loane, E. J. Kirkland, J. Silcox, Visibility of single heavy atoms on thin crystalline silicon in simulated annular dark-field STEM images, Acta Crystallographica A 44 (1988) 912–927.
[44] D. Van Dyck, M. Op de Beeck, A simple intuitive theory for electron diffraction, Ultramicroscopy 64 (1996) 99–107.
[45] K. E. MacArthur, A. J. D'Alfonso, D. Ozkaya, L. Allen, P. Nellist, Optimal ADF STEM imaging parameters for tilt-robust image quantification, Ultramicroscopy 156 (2015) 1–8.
[46] D. Garcia-Gutierrez, C. Gutierrez-Wing, M. Miki-Yoshida, M. Jose-Yacaman, HAADF study of Au-Pt core-shell bimetallic nanoparticles, Applied Physics A 79 (2004) 481–487.
[47] Z. Yu, D. A. Muller, J. Silcox, Effects of specimen tilt in ADF-STEM imaging of a-Si/c-Si interfaces, Ultramicroscopy 108 (2008) 494–501.
[48] C. Langlois, Z. W. Wang, D. Pearmain, C. Ricolleau, Z. Y. Li, HAADF-STEM imaging of CuAg core-shell nanoparticles, Journal of Physics: Conference Series 241 (2010) 012043.
[49] A. J. den Dekker, S. Van Aert, A. van den Bos, D. Van Dyck, Maximum likelihood estimation of structure parameters from high resolution electron microscopy images. Part I: A theoretical framework, Ultramicroscopy 104 (2005) 83–106.
[50] S. Van Aert, A. J. den Dekker, A. van den Bos, D. Van Dyck, J. H. Chen, Maximum likelihood estimation of structure parameters from high resolution electron microscopy images. Part II: A practical example, Ultramicroscopy 104 (2005) 83–106.
[51] D. Van Dyck, Is the frozen phonon model adequate to describe inelastic phonon scattering?, Ultramicroscopy 109 (2009) 677–682.
[52] I. Lobato, D. Van Dyck, An accurate parameterization for the scattering factors, electron densities and electrostatic potentials for neutral atoms that obey all physical constraints, Acta Crystallographica Section A 70 (2014) 636–649.
[53] I. Lobato, S. Van Aert, J. Verbeeck, Progress and new advances in simulating electron microscopy datasets using MULTEM, Ultramicroscopy 168 (2016) 17–27.
[54] D. Zhou, K. Müller-Caspary, W. Sigle, F. F. Krause, A. Rosenauer, P. A. van Aken, Sample tilt effects on atom column position determination in ABF-STEM imaging, Ultramicroscopy 160 (2016) 110–117.
[55] P. Gao, A. Kumamoto, R. Ishikawa, N. Lugg, N. Shibata, Y. Ikuhara, Picometer-scale atom position analysis in annular bright-field STEM imaging, Ultramicroscopy 184 (2018) 177–187.
[56] J. Fatermans, A. J. den Dekker, K. Müller-Caspary, N. Gauquelin, J. Verbeeck, S. Van Aert, Atom column detection from simultaneously acquired ABF and ADF STEM images, Ultramicroscopy 219 (2020) 113046.
[57] A. van den Bos, Parameter Estimation for Scientists and Engineers, John Wiley and Sons, inc., 2007.
[58] P. Magni, G. Sparacino, Modelling Methodology for Physiology and Medicine (Second Edition); 5 - Parameter Estimation, 2014.
[59] H. X. Gao, L.-M. Peng, Parameterization of the temperature dependence of the Debye–Waller factors, Acta Crystallographica Section A 55 (1999) 926–932.